AMERICAN
METEOROLOGICAL
SOCIETY

Journal of Physical Oceanography

The DOI for this manuscript is doi: 10.1175/2010JPO4497.1

On the calculation of available potential energy in internal wave fields

Dujuan Kang * and Oliver Fringer

Department of Civil and Environmental Engineering, Stanford University, Stanford, California

* *Corresponding author address:* Dujuan Kang, Department of Civil and Environmental Engineering, Stanford University, Stanford, CA 94305.

E-mail: kangdj@stanford.edu

ABSTRACT

A comparison of three common formulations for calculating the available potential energy (APE) in internal wave fields is presented, namely the perturbation APE, APE_1, the exact local APE, APE_2, and its approximation for linear stratification, APE_3. The relationship among these formulations is illustrated through a graphical interpretation and a derivation of the energy conservation laws. Numerical simulations are carried out to quantitatively assess the performance of each APE under the influence of different nonlinear and nonhydrostatic effects. The results show that APE_2 is the most attractive in evaluating the local APE, especially for nonlinear internal waves, since use of APE_2 introduces the smallest errors when computing the energy conservation laws. Larger errors arise when using APE_1 because of the large disparity in magnitude between the kinetic energy and APE_1. We show that the disparity in the tendency of APE_1 is compensated by a large flux arising from the reference pressure and density fields. Because the tendency of the kinetic energy is close to that of APE_3, computational errors arise when using APE_3 only in the presence of nonlinear stratification, and these errors increase for stronger flow nonlinearity.

1. Introduction

Not all potential energy can be converted into kinetic energy, which ultimately contributes to mixing. The small active portion of the potential energy that is available for this conversion is referred to as the available potential energy (APE). The concept of APE has been widely used to study the energetics of internal waves (Klymak and Moum 2003; Venayagamoorthy and Fringer 2005; Klymak et al. 2006; Scotti et al. 2006; Lamb 2007; Moum et al. 2007; Carter et al. 2008; Lamb and Nguyen 2009) and other mixing processes in stratified fluids (Winters et al. 1995; Huang 1998; Molemaker and McWilliams 2010).

The domain-integrated APE for an incompressible fluid is defined as the difference in the potential energy between the perturbed state and the reference state, which is the minimum potential energy state obtained through adiabatic processes (Lorenz 1955). Following this definition, different formulations of the APE density have been employed. A classic definition is the perturbation potential energy density $APE_1 = \rho' g z$, where ρ' is the perturbation density, which has been widely used to calculate the depth-integrated (Venayagamoorthy and Fringer 2005; Moum et al. 2007) or domain-integrated APE (Klymak and Moum 2003; Klymak et al. 2006) in analyzing internal wave energetics. Another well-known expression for the APE density is $APE_3 = \rho_0 N^2 \zeta^2/2 = g^2 \rho'^2/2\rho_0 N^2$, where ρ_0 is the constant reference density associated with the Boussinesq approximation, ζ is the vertical displacement of a fluid particle and N is the buoyancy frequency (Gill 1982; Kundu 1990). Although APE_3 is derived from linear theory, it is commonly used for internal wave calculations in which the stratification is slowly-varying (Carter et al. 2008). A positive-definite expression for arbitrary stratifications was proposed by Holliday and McIntyre (1981) as

$APE_2 = \int_{z-\zeta}^{z} g[\rho(z) - \rho_r(z')]dz'$, where ρ_r is the reference density. More recently, this formulation was employed in analyzing the energetics of nonlinear internal waves (Scotti et al. 2006; Lamb 2007; Lamb and Nguyen 2009). Lamb (2008) compared the calculation of APE_1 and APE_2 for an isolated perturbation and pointed out that their integrals over a finite domain are identical.

Typically, when assessing the energy flux budget for a linear, hydrostatic wave, only the dominant kinetic energy flux term $\mathbf{u}p'$ is calculated, where p' is the perturbation hydrostatic pressure (Kunze et al. 2002; Merrifield and Holloway 2002; Nash et al. 2005). However, in the presence of strong nonlinear and nonhydrostatic effects, it is important to include the nonlinear and nonhydrostatic terms in the kinetic energy flux as well as the APE flux term (Venayagamoorthy and Fringer 2005; Lamb 2007; Moum et al. 2007). Therefore, an appropriate evaluation of the APE has important ramifications for analyses of internal wave energetics. In this paper, we provide a comparison of these three formulations for calculating the APE in internal wave fields. Both theoretical analysis and numerical simulations are employed to highlight their differences. In particular, we compare their performance in the numerical simulations under different nonlinear and nonhydrostatic conditions. Advantages and limitations of each formulation in analyzing the energetics of internal waves are discussed.

2. Interpretation of APE

We consider a stratified incompressible fluid with a stable reference stratification $\rho_r(z)$. The buoyancy frequency is defined by $N^2(z) = -\frac{g}{\rho_0}\frac{d\rho_r}{dz}$. Figure 1 shows the vertical distribution of the reference density $\rho_r(z)$ and the perturbed density $\rho(x, y, z, t) = \rho_r(z) + \rho'(x, y, z, t)$

for a horizontal location (x, y) and time t. When perturbed, a fluid particle experiences a vertical displacement $\zeta = z - z_*$, moving from $z_*(x, y, z, t)$ in the reference state to z in the perturbed state. As a result, the density of the fluid parcel must satisfy $\rho(x, y, z, t) = \rho_r(z_*)$. The APE densities at point $D(x, y, z, t)$ in Figure 1 can be interpreted graphically in terms of areas as

$$APE_1 = \rho' g z = g \times Area(AEFD)\,, \tag{1}$$

$$APE_2 = \int_{z_*}^{z} g\,[\rho(z) - \rho_r(z')]\,dz' = g \times Area(ACD)\,, \tag{2}$$

where $Area(ACD)$ is the lightly-shaded region in Figure 1. Because the portion of the potential energy between the perturbed and the reference density profiles is the true active potential energy, or the energy that is available for conversion to kinetic energy, APE_2 is an exact expression to evaluate the local APE (Holliday and McIntyre 1981; Shepherd 1993; Lamb 2007, 2008). APE_1 includes some area associated with the inactive portion of the potential energy and thus is larger in magnitude than the kinetic energy. Furthermore, APE_1 is coordinate dependent since its value depends on the height at which $z = 0$. Therefore, APE_1 is not a good choice to evaluate APE on a local basis. A coordinate-independent formulation of APE_1, given by $\rho g \zeta = g \times Area(GHCD)$, was used by Winters et al. (1995) to obtain the volume-integrated APE.

Using the Taylor series expansion in powers of ρ', APE_2 can be expressed as

$$APE_2 = \frac{g^2 \rho'^2}{2\rho_0 N^2} + \frac{g^3 (N^2)_z \rho'^3}{6\rho_0^2 N^6} + O(\rho'^4)\,. \tag{3}$$

If the fluid is linearly stratified (with constant N), only the leading term on the right-hand

side of equation (3) remains. In this limit we obtain

$$APE_3 \;=\; \frac{g^2\rho'^2}{2\rho_0 N^2} = APE_2 + err_3\,. \tag{4}$$

This expression is the well-known linear APE density (Gill 1982; Kundu 1990). For nonlinear stratifications, APE_3 is not an exact expression of the APE density and differs to leading order by an amount that can be estimated by the second term on the right hand side of equation (3). Graphically, APE_3 can be interpreted as g times the area of triangle (ACD) in Figure 1. The dark shaded region is err_3, which vanishes for linear stratification.

3. Energy conservation laws

For an inviscid, non-diffusive, Boussinesq fluid, the evolution equations for the kinetic energy density $KE = \rho_0 \mathbf{u}\cdot\mathbf{u}/2$ and the potential energy density $PE = \rho g z$ are given by

$$\frac{\partial KE}{\partial t} + \nabla\cdot\underbrace{\left[\mathbf{u}\left(KE + p_{nh} + p' + p_s + p_r\right)\right]}_{\mathbf{F}_k} \;=\; -\rho g w\,, \tag{5}$$

$$\frac{\partial PE}{\partial t} + \nabla\cdot\underbrace{\left(\mathbf{u}PE\right)}_{\mathbf{F}_p} \;=\; \rho g w\,, \tag{6}$$

where the pressure is split into its hydrostatic and nonhydrostatic components with $p = p_h + p_{nh}$. The hydrostatic pressure is further decomposed as $p_h = p_r(z) + p'(x,y,z,t) + p_s(x,y,t)$, with p_s the free-surface pressure. Using the rigid-lid approximation, the reference pressure is $p_r = g\int_z^0 \rho_r\, dz'$ and the perturbation hydrostatic pressure is $p' = g\int_z^0 \rho'\, dz'$. Summing the above two energy equations gives the total energy conservation law as

$$\frac{\partial (KE + PE)}{\partial t} + \nabla\cdot\left[\mathbf{u}\left(KE + PE + p_{nh} + p' + p_s + p_r\right)\right] = 0\,. \tag{7}$$

These energy equations show that energy is transferred into and out of a particular control volume via the kinetic energy flux $\mathbf{F}_k$ and the potential energy flux $\mathbf{F}_p$, while within the control volume energy is converted between PE and KE via the buoyancy flux $-\rho g w$. This energy budget is illustrated by the solid arrows in Figure 2.

We now consider the energy budget between the active energy components. Based on the definition of each APE density, and along with the expression of p_r, we obtain the KE and PE equations with active energy fluxes as

$$\frac{\partial KE}{\partial t} + \nabla \cdot \underbrace{[\mathbf{u}\,(KE + p_{nh} + p' + p_s)]}_{\mathbf{F}'_k} = -\rho' g w\,, \tag{8}$$

$$\frac{\partial APE}{\partial t} + \nabla \cdot \underbrace{[\mathbf{u}\,(APE + f)]}_{\mathbf{F}'_p} = \rho' g w\,, \tag{9}$$

where $\mathbf{F}'_k = \mathbf{F}_k - \mathbf{u}p_r$ is the active kinetic energy flux because it excludes work done by the reference pressure from the total kinetic energy flux. The function f is defined as

$$f = \begin{cases} p_r + \rho_r g z\,, & \text{for } APE_1 \\ 0\,, & \text{for } APE_2 \\ 0\,, & \text{for } APE_3 \text{ with linear } \rho_r\,. \end{cases} \tag{10}$$

For APE_2, the available potential energy flux $\mathbf{F}'_p$ is just $\mathbf{u}APE_2$ which is the truly active potential energy flux, while for APE_1, a reference energy flux term $\mathbf{u}f$ is included, which can be much larger than the active energy flux terms given $\rho_r \gg \rho'$ (Venayagamoorthy and Fringer 2005). For APE_3 in nonlinear-stratified fluids, equation (9) does not hold due to the error discussed in Section 2, which requires inclusion of the term $\partial(err_3)/\partial t$ on the right-hand side of equation (9) to ensure a balance. The energy conservation between the active components is obtained by taking the sum of (8) and (9) to give

$$\frac{\partial (KE + APE_n)}{\partial t} + \nabla \cdot [\mathbf{u}\,(KE + APE_n + p_{nh} + p' + p_s + f)] = 0\,. \tag{11}$$

The dashed arrows in Figure 2 illustrate the energy transfer and conversion via the active energy fluxes. Equations (8)-(11) show that the conservation laws for APE_2 are independent of the reference state and thus appropriately describe the energy transfer between the kinetic energy and the available potential energy.

4. Energetics of progressive internal waves

a. Numerical setup

We study the evolution of a first-mode internal wave over flat, frictionless topography in a two-dimensional $(x-z)$ domain of length $L = 2\lambda$ and depth D, where λ is the wavelength. Periodic boundary conditions are imposed in the direction of wave propagation, which effectively extends the domain to an infinite length in the x-direction. Numerical simulations are performed using the SUNTANS code of Fringer et al. (2006) to assess the influence of the stratification, nonlinearity, and nonhydrostatic effects on different APE formulations.

Two different initial reference stratifications are considered, namely linear stratification given by $\rho_r(z) = \rho_0 - \Delta\rho_1(z/D)$, and nonlinear stratification given by $\rho_r(z) = \rho_0 - \Delta\rho_2[\tanh(5z/D + 1) - \tanh(1)]$, where $\rho_0 = 1000$ kg m^{-3}. We assume a first-mode internal wave phase speed $c_1 = 1$ m s^{-1}, a depth $D = 500$ m and a wavelength $\lambda = 50$ km, which requires $\Delta\rho_1 = 2.01$ kg m^{-3} and $\Delta\rho_2 = 1.01$ kg m^{-3}. To assess the influence of internal wave nonlinearity, for each stratification we consider two different Froude numbers, namely $Fr = u_0/c_1 = 0.05$ and $Fr = 0.2$, where u_0 is the horizontal velocity amplitude. Nonhydrostatic effects are assessed by shortening the wavelength to $\lambda = 2$ km so that $\lambda/D = 4$, which

is more nonhydrostatic than the longer wave case which has $\lambda/D = 100$. With $\lambda/D = 4$ we set $Fr = 0.2$ and perform two additional simulations using the linear and nonlinear stratifications. In total, there are six simulations, represented by the results in each column of Table 1.

b. Evolution of first-mode internal waves

The upper three panels (a)-(c) in Figure 3 depict a time sequence of the evolution of waves with a fixed Froude number $Fr = 0.2$ but with different stratifications and aspect ratios λ/D. Despite having the same Froude number, the wave in the linear stratification (Figure 3(a)) does not steepen into a train of rank-ordered solitary-like waves as it does in the nonlinear stratification as shown in Figure 3(b). Although both waves travel at the same linear phase speed, isopycnal displacements for the nonlinear stratification have a stronger effect on the amplitude dispersion of the wave, thereby causing nonlinear steepening. This effect can be reduced by increasing the relative importance of the nonhydrostatic pressure (Figure 3(c)). Decreasing the value of λ/D increases the relative effect of the nonhydrostatic pressure, thereby reducing the rate at which the waves steepen.

c. Energetics

In practice, the depth- and volume-integrated energy budgets are of primary interest, particularly for internal waves. In what follows we focus on the depth-integrated budget, and we note that a similar analysis was performed for the volume-integrated budget that yielded identical results. The depth-integration of the left-hand side of equations (8) and

(9) are represented by $\overline{sumKE'}$ and $\overline{sumAPE}$, respectively. Here $\overline{()}$ represents the depth-integration of a quantity, while *sum* stands for the summation of all terms on the left-hand side of an equation. Using this notation, we must have

$$-\overline{sumKE'}(x,t) = \overline{sumAPE}(x,t) = \overline{\rho' g w}(x,t)\,, \tag{12}$$

which holds for all APE formulations except for APE_3 in the presence of nonlinear stratification. The lower three panels (d)-(f) in Figure 3 illustrate this balance relation as a function of time t/T at $x = \lambda$ for APE_2. On each panel, three curves representing normalized $\overline{\rho' g w}$, $-\overline{sumKE'}$, and $\overline{sumAPE_2}$ are indistinguishable, implying a precise balance given by (12).

A quantitative measure of the imbalance in computing equation (12) is given by

$$Imb_n(x) = \frac{\text{std}\left[\overline{sumAPE_n}(x,t) - \overline{\rho' g w}(x,t)\right]}{\text{std}\left[\overline{\rho' g w}(x,t)\right]}\,, \tag{13}$$

where $n = 1, 2, 3$, and std() represents the standard deviation of a quantity over the first six wave periods. The results at $x = \lambda$ are presented in Table 1. Errors are incurred both due to the theoretical imbalance when using APE_3 and from computational errors when solving the equations on discrete grid. In general, APE_2 performs the best, although it yields a larger imbalance than APE_3 in linear stratification due to numerical errors in computing z_* on a discrete grid. As expected, in the presence of nonlinear stratification APE_3 does not satisfy equation (9) and thus shows significant imbalance. Although in theory APE_1 should satisfy the balance relation (12) well, it demonstrates relatively large imbalances, which cannot be improved (in a relative sense) with more numerical accuracy. The numerical imbalance for APE_1 is larger than that for APE_2 because small errors in computing ρ' are magnified for $APE_1 = \rho' g z$ relative to $APE_2 \sim \rho' g \zeta$ since, in general, $z >> \zeta$. A comparison of the energy

balance (12) for different APE formulations is shown in Figure 4 for the case with nonlinear ρ_r, $\lambda/D = 100$, and $Fr = 0.2$.

For the same case as in Figure 4, Figure 5 (a) compares the tendency terms of KE and APE. $\overline{\partial APE_1/\partial t}$ is roughly one order of magnitude larger than $\overline{\partial KE/\partial t}$. While for APE_2 and APE_3, the tendency terms of APE and KE are of the same order of magnitude. Figure 5(b) presents the contributions from all terms in equation (9) for APE_1. The reference energy flux term $\overline{\nabla \cdot (\mathbf{u}f)}$, although having little physical significance, is roughly one order of magnitude larger than the active energy flux term $\overline{\nabla \cdot (\mathbf{u}APE_1)}$. This large reference energy flux compensates the large tendency of APE_1 in the conservation law. These results show how APE_1 does not represent the exact local APE and highlight the role of the $\overline{\nabla \cdot (\mathbf{u}f)}$ term in evaluating the true energy flux budget for APE_1.

5. Conclusions

We have compared three different APE formulations and assessed their performance in numerical simulations of a progressive internal wave under different nonlinear and nonhydrostatic conditions. A theoretical analysis and numerical simulations clearly show that APE_2 (and APE_3 in the presence of linear stratification) is more attractive in evaluating the local APE because the size and tendency of APE_2 are of the same order of magnitude as those of KE, while the size and tendency of APE_1 are much larger. The disparity in the tendency is compensated by the presence of a large reference energy flux term $\mathbf{u}f$ in the conservation law for APE_1. In computing the conservation laws, the imbalance for APE_1 is related to its large tendency term and the large reference energy flux term which accentuate numerical

errors. While the imbalance for APE_3 is related to the nonlinearity of the stratification, and the errors increase for stronger internal wave nonlinearity. Overall, APE_2 shows the best numerical performance in computing the conservation laws, particularly for nonlinear and nonhydrostatic cases.

Acknowledgments.

The authors gratefully acknowledge the support of ONR Grant N00014-05-1-0294. The helpful discussions with Dr. Rocky Geyer, Dr. Alan Blumberg and Dr. Karan Venayagamoorthy are greatly appreciated. We also thank three anonymous reviewers for their valuable comments and suggestions.

REFERENCES

Carter, G. S., et al., 2008: Energetics of m2 barotropic-to-baroclinic tidal conversion at the hawaiian islands. *J. Phys. Oceanogr.*, **38**, 2205–2223.

Fringer, O. B., M. Gerritsen, and R. L. Street, 2006: An unstructured-grid, finite-volume, nonhydrostatic, parallel coastal ocean simulator. *Ocean Modelling*, **14**, 139–278.

Gill, A. E., 1982: *Atmosphere-Ocean Dynamics*. Academic Press.

Holliday, D. and M. E. McIntyre, 1981: On potential energy density in an incompressible, stratified fluid. *J. Fluid Mech.*, **107**, 221–225.

Huang, R. X., 1998: Mixing and available potential energy in a boussinesq ocean. *J. Phys. Oceanogr.*, **28**, 669–678.

Klymak, J. M. and J. N. Moum, 2003: Internal solitary waves of elevation advancing on a shoaling shelf. *Geophys. Res. Lett.*, **30(20)**, 2045, doi:10.1029/2003GL017 706.

Klymak, J. M., R. Pinkel, C.-T. Liu, A. K. Liu, and L. David, 2006: Prototypical solitons in the south china sea. *Geophys. Res. Lett.*, **33**, L11 607, doi:10.1029/2006GL025 932.

Kundu, P. K., 1990: *Fluid Mechanics*. Academic Press.

Kunze, E., L. K. Rosenfeld, G. S. Carter, and M. C. Gregg, 2002: Internal waves in monterey submarine canyon. *J. Phys. Oceanogr.*, **32**, 1890–1913.

Lamb, K. G., 2007: Energy and pseudoenergy flux in the internal wave field generated by tidal flow over topography. *Cont. Shelf Res.*, **27**, 1208–232.

Lamb, K. G., 2008: On the calculation of the available potential energy of an isolated perturbation in a density-stratified fluid. *J. Fluid Mech.*, **597**, 415–427.

Lamb, K. G. and V. T. Nguyen, 2009: Calculating energy flux in internal solitary waves with an application to reflectance. *J. Phys. Oceanogr.*, **39**, 559–580.

Lorenz, E. N., 1955: Available potential energy and the maintenance of the general circulation. *Tellus*, **7**, 157–167.

Merrifield, M. A. and P. E. Holloway, 2002: Model estimates of m2 internal tide energetics at the hawaiian ridge. *J. Geophys. Res.*, **107**, 3179, doi:10.1029/2001JC000 996.

Molemaker, M. J. and J. C. McWilliams, 2010: Local balance and cross-scale flux of available potential energy. *J. Fluid Mech.*, **645**, 295–314.

Moum, J. N., J. M. Klymak, J. D. Nash, A. Perlin, and W. D. Smyth, 2007: Energy transport by nonlinear internal waves. *J. Phys. Oceanogr.*, **37**, 1968–1988.

Nash, J. D., M. H. Alford, and E. Kunze, 2005: Estimating internal wave energy fluxes in the ocean. *J. Atmos. Ocean. Tech.*, **22**, 1551–1570.

Scotti, A., R. Beardsley, and B. Butman, 2006: On the interpretation of energy and energy fluxes of nonlinear internal waves: an example from massachusetts bay. *J. Fluid Mech.*, **561**, 103–112.

Shepherd, T., 1993: A unified theory of available potential energy. *Atmos. Oceans*, **31**, 1–26.

Venayagamoorthy, S. K. and O. B. Fringer, 2005: Nonhydrostatic and nonlinear contributions to the energy flux budget in nonlinear internal waves. *Geophys. Res. Lett.*, **32**, L15 603, doi:10.1029/2005GL023 432.

Winters, K. B., P. N. Lombard, J. J. Riley, and E. A. D'Asaro, 1995: Available potential energy and mixing in stratified fluids. *J. Fluid Mech.*, **289**, 115–128.

List of Tables

1 Comparison of the imbalance of equation (12) at x=λ for the three APE formulations under different conditions. 15

TABLE 1. Comparison of the imbalance of equation (12) at x=λ for the three APE formulations under different conditions.

	linear ρ_b, λ/D=100		nonlinear ρ_b, λ/D=100		nonlinear ρ_b, λ/D=4	
	Fr=0.05	Fr=0.2	Fr=0.05	Fr=0.2	Fr=0.05	Fr=0.2
Imb_1	0.0019	0.0025	0.0092	0.0529	0.0038	0.0065
Imb_2	0.0016	0.0015	0.0052	0.0241	0.0036	0.0064
Imb_3	0.0014	0.0014	0.0209	0.1220	0.0171	0.0377

List of Figures

1 Schematic diagram depicting the different formulations of the APE density. The rectangular area $AEFD$ stands for APE_1, the light shaded area ACD represents APE_2, while the triangle area ACD stands for APE_3. The dark shaded area is err_3, the difference between APE_2 and APE_3. 18

2 Diagram of the energy budget for adiabatic, Boussinesq flow. Solid arrow lines: traditional energy flux budget; dashed arrow lines: active energy flux budget. 19

3 Evolution of a first-mode internal wave under different conditions: (a) linear ρ_r, $\lambda/D = 100$; (b) nonlinear ρ_r, $\lambda/D = 100$; (c) nonlinear ρ_r, $\lambda/D = 4$. The linear phase speed $c_1 = 1$ m s^{-1} and $Fr = 0.2$ for all three cases. In each upper panel the four color plots show the distributions of $\rho - \rho_0$ at t/T =0, 1, 2, and 3. The lower panels (d)-(f) show the corresponding energy balance (12) as a function of time t/T at $x = \lambda$. In each of the lower panels, there are three indistinguishable curves $\overline{\rho' g w}$ (solid), $-\overline{sumKE'}$ (dashed), and $\overline{sumAPE_2}$ (dots), all normalized by the maximum value of $\overline{\rho' g w}$ over the first three wave periods. 20

4 Comparison of the energy balance (12) for different APE formulations as a function of t/T at $x = \lambda$. The embedded plot is a zoomed-in view to provide more detail. This case is with nonlinear ρ_r, $\lambda/D = 100$, and $Fr = 0.2$. All terms are normalized by the maximum value of $\overline{\rho' g w}$ over the first three wave periods. 21

5 Comparison of the tendency of the kinetic energy and the three APE (a) and comparison of the depth-integrated terms in the APE equation (9) for $APE = APE_1$ (b). The simulation parameters and the value for normalization are the same as those in Figure 4. 22

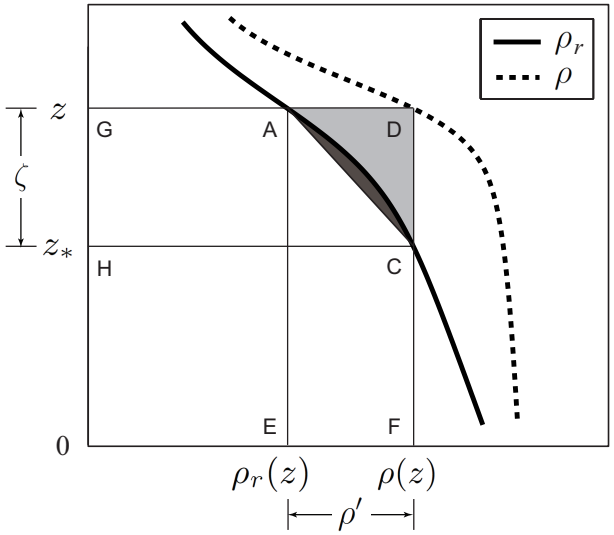

FIG. 1. Schematic diagram depicting the different formulations of the APE density. The rectangular area $AEFD$ stands for APE_1, the light shaded area ACD represents APE_2, while the triangle area ACD stands for APE_3. The dark shaded area is err_3, the difference between APE_2 and APE_3.

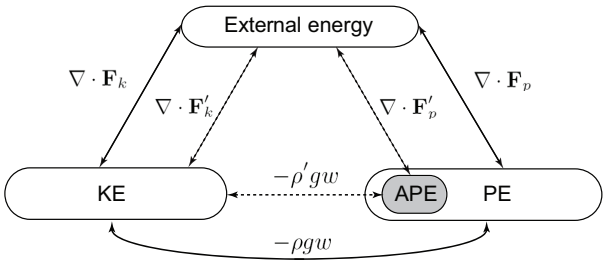

FIG. 2. Diagram of the energy budget for adiabatic, Boussinesq flow. Solid arrow lines: traditional energy flux budget; dashed arrow lines: active energy flux budget.

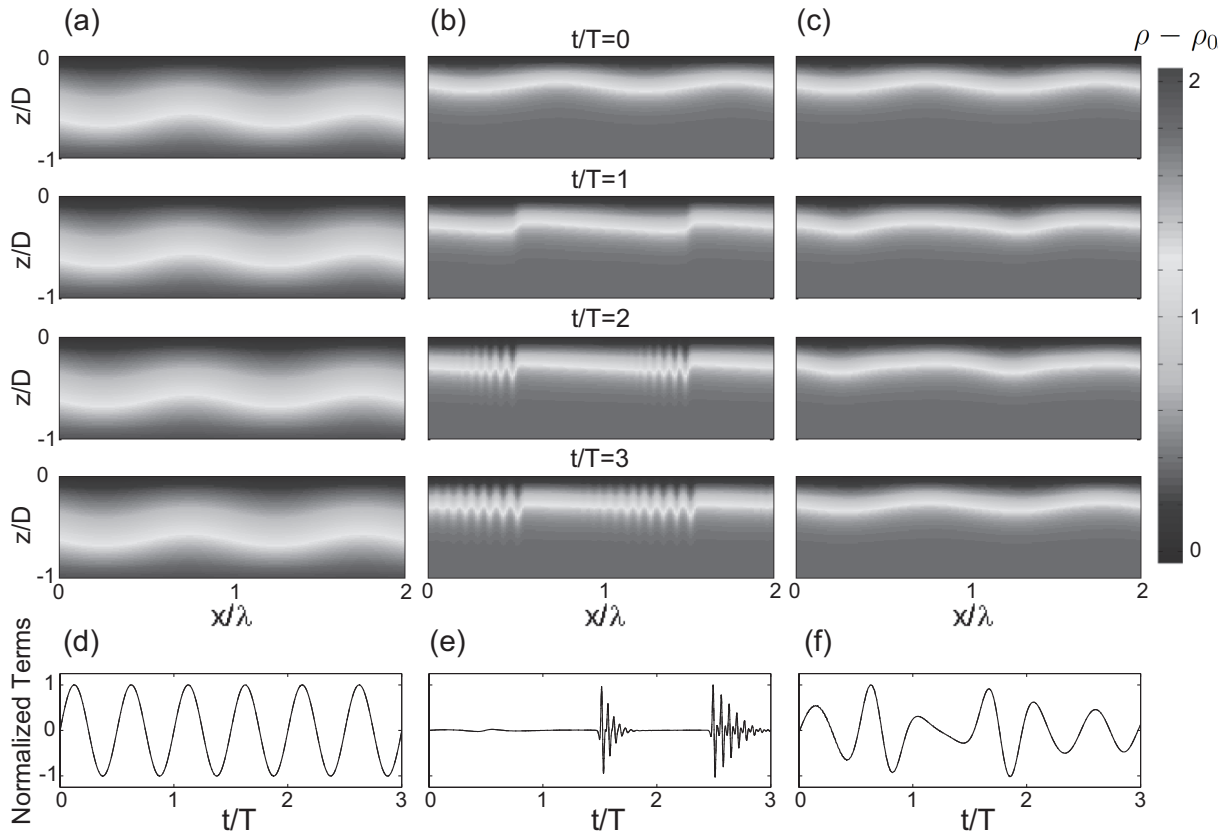

FIG. 3. Evolution of a first-mode internal wave under different conditions: (a) linear ρ_r, $\lambda/D = 100$; (b) nonlinear ρ_r, $\lambda/D = 100$; (c) nonlinear ρ_r, $\lambda/D = 4$. The linear phase speed $c_1 = 1$ m s^{-1} and $Fr = 0.2$ for all three cases. In each upper panel the four color plots show the distributions of $\rho - \rho_0$ at t/T =0, 1, 2, and 3. The lower panels (d)-(f) show the corresponding energy balance (12) as a function of time t/T at $x = \lambda$. In each of the lower panels, there are three indistinguishable curves $\overline{\rho' g w}$ (solid), $-\overline{sumKE'}$ (dashed), and $\overline{sumAPE_2}$ (dots), all normalized by the maximum value of $\overline{\rho' g w}$ over the first three wave periods.

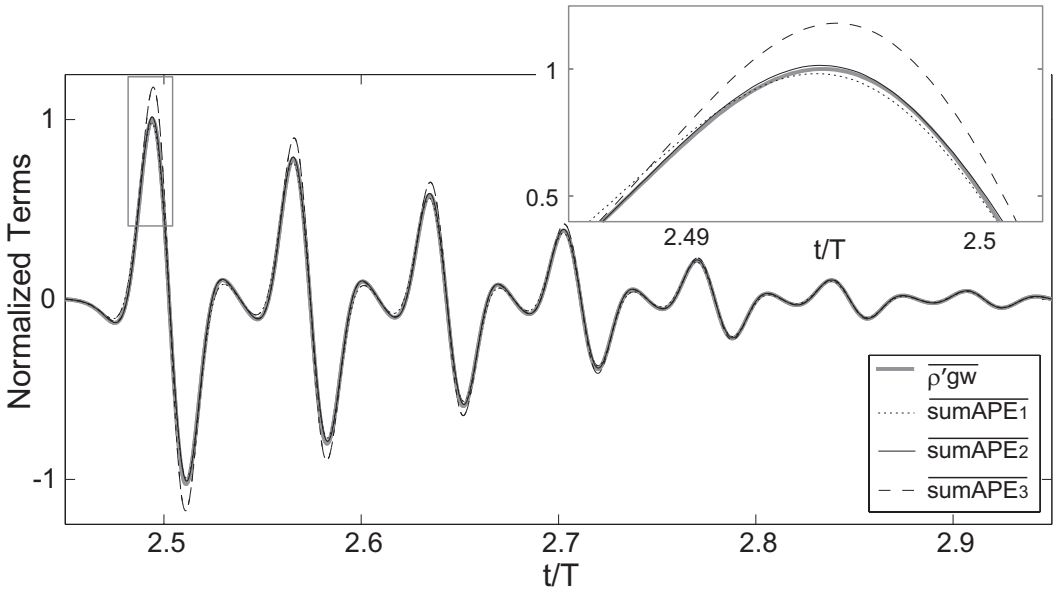

FIG. 4. Comparison of the energy balance (12) for different APE formulations as a function of t/T at $x = \lambda$. The embedded plot is a zoomed-in view to provide more detail. This case is with nonlinear ρ_r, $\lambda/D = 100$, and $Fr = 0.2$. All terms are normalized by the maximum value of $\overline{\rho' g w}$ over the first three wave periods.

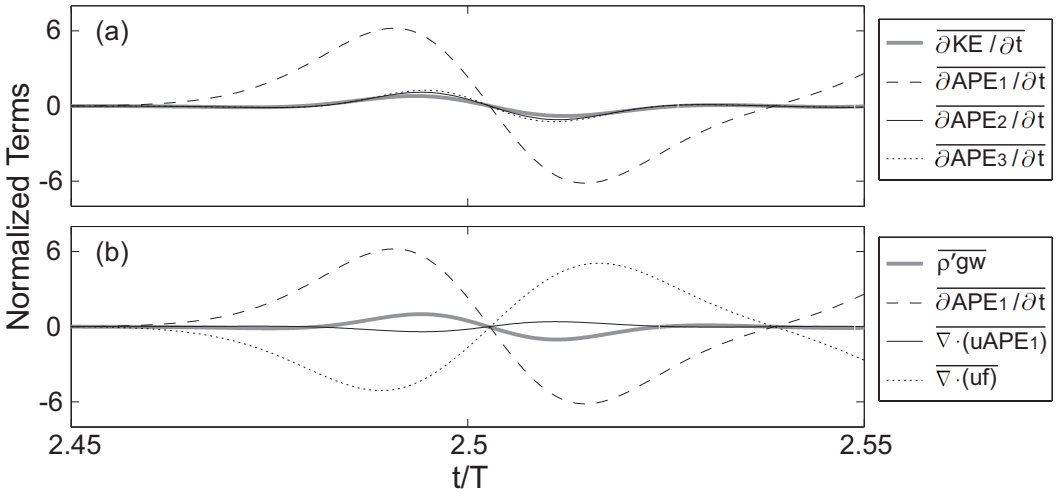

FIG. 5. Comparison of the tendency of the kinetic energy and the three APE (a) and comparison of the depth-integrated terms in the APE equation (9) for $APE = APE_1$ (b). The simulation parameters and the value for normalization are the same as those in Figure 4.